Phase Diagram of Kob-Andersen-Type Binary Lennard-Jones Mixtures

Ulf R. Pedersen,[*] Thomas B. Schrøder, and Jeppe C. Dyre
Glass and Time, IMFUFA, Department of Science and Environment, Roskilde University,
P.O. Box 260, DK-4000 Roskilde, Denmark

The binary Kob-Andersen (KA) Lennard-Jones mixture is the standard model for computational studies of viscous liquids and the glass transition. For very long simulations, the viscous KA system crystallizes, however, by phase separating into a pure A particle phase forming a fcc crystal. We present the thermodynamic phase diagram for KA-type mixtures consisting of up to 50% small (B) particles showing, in particular, that the melting temperature of the standard KA system at liquid density 1.2 is 1.028(3) in A particle Lennard-Jones units. At large B particle concentrations, the system crystallizes into the CsCl crystal structure. The eutectic corresponding to the fcc and CsCl structures is cutoff in a narrow interval of B particle concentrations around 26% at which the bipyramidal orthorhombic PuBr$_3$ structure is the thermodynamically stable phase. The melting temperature's variation with B particle concentration at two constant pressures, as well as at the constant density 1.2, is estimated from simulations at pressure 10.19 using isomorph theory. Our data demonstrate approximate identity between the melting temperature and the onset temperature below which viscous dynamics appears. Finally, the nature of the solid-liquid interface is briefly discussed.

Standard models are invaluable in physics by providing well-understood reference systems for testing new ideas. Well-known examples are the ideal gas model, the Ising model for critical phenomena [1,2], and the ϕ^4 scalar field theory for renormalization [1,3]. In computational studies of viscous liquids and the glass transition [4–9], the Kob-Andersen (KA) binary Lennard-Jones (LJ) mixture has been the standard model for 20 years [10]. The KA model is a mixture of 80% large A particles and 20% small B particles. The model is characterized by a strong AB attraction, which disfavors phase separation into a pure A phase by making it energetically costly. When the model crystallizes in very long computer runs, this nevertheless happens by phase separation into a pure A phase forming a face-centered cubic (fcc) crystalline structure [11,12]. This may be contrasted with the Wahnström 50/50 binary LJ mixture [13], which has a much more complex crystal structure [14].

In the KA mixture, all particles have the same mass and interact via LJ pair potentials $v(r) = 4\varepsilon[(r/\sigma)^{-12} - (r/\sigma)^{-6}]$ truncated and shifted to zero at 2.5σ with $\sigma_{BB}/\sigma_{AA} = 0.88$, $\sigma_{AB}/\sigma_{AA} = 0.8$, $\varepsilon_{BB}/\varepsilon_{AA} = 0.5$, and $\varepsilon_{AB}/\varepsilon_{AA} = 1.5$. The large ε_{AB} favors stability toward phase separation. The parameters of the KA model were chosen to mimic the nickel-phosphor mixture [10] that has a eutectic at 20% P atoms [15]; eutectic mixtures [16] are generally regarded as optimal for glass formation [17].

Crystallization of binary LJ models has been simulated by several groups [18–21]. In 2001, Wales and co-workers showed that the KA system possesses low-lying crystalline minima [22], confirming the prevailing view that the KA

viscous liquid is not in true thermodynamic equilibrium [23]. Two years later, Fernandez and Harrowell reported rapid crystal growth for the 50/50 KA mixture [24] and argued that, for general KA-type mixtures, the lowest-energy ordered state consists of coexisting phases of single-component fcc and equimolar CsCl crystal structures [25]. In 2009, Kob and co-workers reported that the standard 80/20 KA mixture crystallizes in two dimensions, whereas the 65/35 composition does not [26]. Royall and co-workers in 2015 showed that locally favored structures impede crystallization if they do not tile space [27]. In 2016, Bhattacharyya and co-workers showed that the entropic penalty for demixing is a nonmonotonic function of composition with a maximum at a composition close to that of the standard KA model [28].

The below study utilized the software packages RUMD [29], LAMMPS [30], VMD [31], and a home-written code [32]. The majority of the simulations involved 8000 particles, and a few had 10 000 particles.

Most KA-model papers focus on density 1.2 in the LJ unit system defined by the A particle parameters. We determined the melting temperature of the standard KA liquid at this density from two-phase simulations by proceeding as follows. First, the pressure of the liquid was calculated as a function of temperature at density 1.2 [Fig. 1(a)]. Next, we determined the lattice parameters of pure A particle fcc crystals at the temperatures and pressures of Fig. 1(a) [33,34]. The final step was to simulate at each temperature and pressure a two-phase system composed initially of half KA liquid and half pure A crystal, choosing a box size compatible
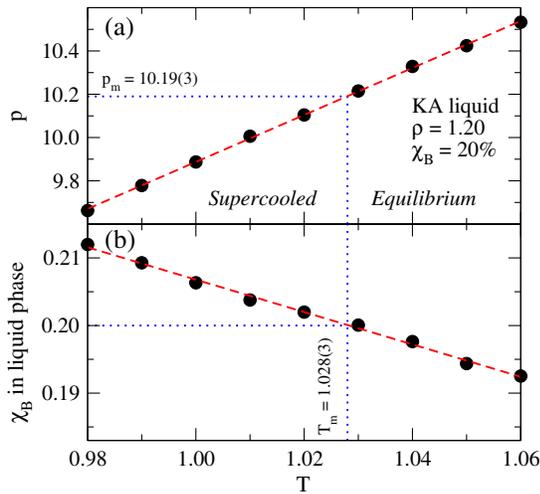
FIG. 1. Determining the standard KA system's melting temperature and pressure when the liquid at coexistence has density 1.2. (a) The pressure of the KA liquid at density 1.2 as a function of temperature. (b) The fraction of B particles in the liquid phase of an equilibrated two-phase simulation at this pressure. The melting temperature of the density 1.2 KA liquid is seen to be given by $T_m = 1.028(3)$ at pressure $p = 10.19(3)$.

with the determined lattice constant and using a "longitudinal" barostat, ensuring constant pressure perpendicular to the crystal-liquid interface. Over time, the pure A crystal either grows or shrinks, which changes the ratio of A to B particles in the liquid phase. When equilibrium has been reached, the temperature is the melting temperature
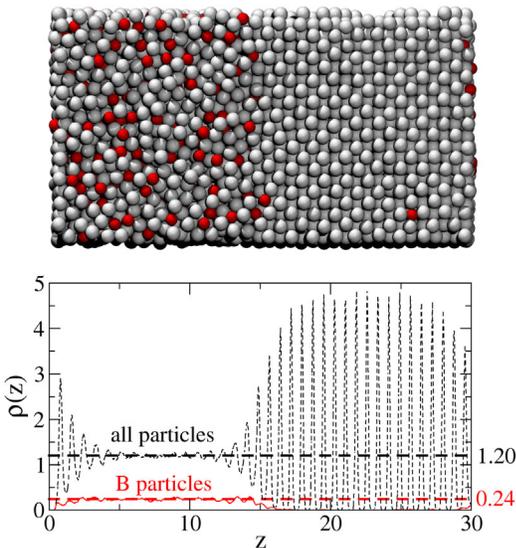
FIG. 2. (Upper) Snapshot of a two-phase simulation in a periodic box at the coexistence temperature 1.028 and pressure $p = 10.19$ (A particle LJ units). A particles are gray and B particles are red. The density of the liquid phase is 1.2. (Lower) Overall density (black dotted line) and B particle density (red line) along the z direction. The fraction of B particles in the liquid phase is 0.24/1.20 = 20%.

of that particular liquid composition [35]. Figure 1(b) shows the fraction of B particles where the abscissa is the melting temperature at the pressure identified in Fig. 1(a). For the standard 80/20 KA system, we see that, at pressure $p = 10.19(3)$ and liquid-phase density 1.2, freezing occurs at the temperature 1.028(3).

Figure 2 shows a snapshot of the two-phase equilibrium KA system at $T = 1.028$ and $p = 10.19$. A few B particles (red) have diffused into the pure A crystal, which is to be expected given the relatively high temperature. The lower panel shows the density of B particles (red) and of all particles (black), confirming that the liquid phase has density 1.2 and contains 20% B particles.

Having determined the pressure of the state point at which the KA liquid at freezing has density 1.2, we proceed to establish the composition-temperature phase diagram at this pressure (Fig. 3). The phase diagram was arrived at by the above method in which the solid-liquid interface is "pinned" due to the composition constraint in the liquid.
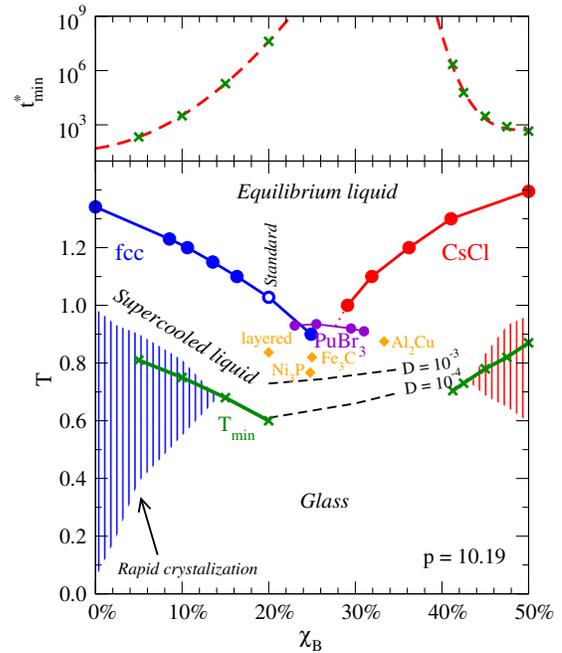
FIG. 3. Phase diagram of KA-type mixtures at pressure $p = 10.19$, where χ_B is the fraction of B particles in the equilibrium liquid phase. The solid blue line shows the melting temperature of the pure A particle fcc crystal, the solid red line shows the melting temperature of the CsCl structure, and the short solid purple line shows the melting temperature of the PuBr$_3$ structure. Orange symbols give the melting temperature of other, less stable structures at selected compositions (see text). The two dashed black lines are isodiffusional lines. The green crosses show the temperature $T_{\min}$ of minimum crystallization time for a given χ_B; the colored regions are where rapid crystallization occurs, defined by $t^* < 2 \times 10^5$ for 8000 particles. (Upper) Minimum crystallization time. Extrapolations based on third-order polynomials (red dashed lines) suggest that the best glass former is at a higher B particle composition than the eutectic.

TABLE I.   State point data for the liquid in coexistence with different crystalline states at pressure $p = 10.19$ at the specified B particle concentrations in the liquid phase (A particle LJ units). Crystal structures are identified by prototype, Hermann-Mauguin space group, and International Union of Crystallography number. T_m is the melting temperature, ρ_s and ρ_l are the solid and liquid densities, u_s and u_l are the average potential energies per particle of the solid and liquid phases, ΔS is the constant-pressure entropy of fusion calculated from the parameters and the phase-equilibrium condition $\Delta G = 0$.

		χ_B^{liquid}	T_m	ρ_s	ρ_l	u_s	u_l	ΔS
fcc	[$Fm\bar{3}m$; 225]	0%	1.341(4)	1.0535	0.9796	−3.6460	−2.7971	1.177
PuBr$_3$	[$Cmcm$; 63]	25.5%	0.935(8)	1.3515	1.2712	−7.1192	−6.3170	1.367
Fe$_3$C	[$Pnma$; 62]	25.0%	0.820(8)	1.3501	1.2950	−7.1446	−6.5360	1.134
Ni$_3$P	[$I\bar{4}$; 82]	24.8%	0.767(6)	1.3582	1.2878	−7.0759	−6.6409	1.102
Al$_2$Cu	[$I\bar{4}/mcm$; 140]	33.4%	0.875(8)	1.4256	1.2858	−7.1720	−6.9785	1.109
CsCl	[$Pm\bar{3}m$; 221]	49.4%	1.394(4)	1.6427	1.4392	−7.5850	−5.9561	1.798

When the liquid has the same composition as the crystal, this constraint is absent, however, in which case we used the interface-pinning method [36].

At small B particle concentrations, the solid phase is a pure A-phase fcc crystal. Upon increasing the B particle concentration, at some point the system crystallizes instead into the 50/50 CsCl structure of two interpenetrating cubic lattices of A and B particles [24,28]. The eutectic of these two crystal phases is located around 26% B particles, but interestingly there is a narrow region around the eutectic in which the bipyramidal orthorhombic PuBr$_3$ structure based on triangular prisms is the thermodynamically stable phase. We also studied the Al$_2$Cu, Fe$_3$C, and Ni$_3$P structures shown by Fernández and Harrowell to be of low energy at $T = 0$ and $p = 0$ [37], but found that their melting temperatures are all lower (compare Fig. 3 and Table I). In Fig. 3, "layered" denotes a structure of alternating layers of CsCl and pure A particle fcc crystals, which is known to have low energy at $T = 0$ [22,24].

To investigate the dynamics of crystallization, we utilized the following protocol for a range of compositions and temperatures ($p = 10.19$): First, one equilibrates up to ten liquid configurations at the coexistence temperature. Subsequently, the temperature is changed to the desired value and one computes the crystallization time t^*, defined as the average time at which 10% of the particles are in a crystalline environment (monitored by the crystal order parameter defined as the absolute value of the density's Fourier transform at the fundamental lattice k vector [38]). The blue and red areas in Fig. 3 are regions with rapid crystallization. As expected, the spontaneously formed crystals are fcc for 0%–15% B's and CsCl for 41%– 50% B's. The green crosses show for each composition the temperature $T_{\min}$ at which the crystallization time is at a minimum, $t^*_{\min}$. The upper panel shows $t^*_{\min}$.

The melting line in Fig. 3 is for $p = 10.19$, the pressure at which the coexisting liquid for the standard 80/20 KA system has density 1.2. The melting temperature's variation with B particle concentration at other pressures or at constant liquid-phase density may be estimated from the $p = 10.19$ results from the fact that the melting line to

a good approximation follows a liquid isomorph [8,39]. The estimate, which makes use of the fact that LJ-type systems are R-simple, i.e., have strong virial potential-energy correlations [40–42], works as follows. For any mixture of LJ particles, if the melting temperature at liquid density ρ_0 is T_0, the melting temperature T at liquid density ρ is approximately given [43,44] by

$$T/T_0 = (\gamma_0/2 - 1)(\rho/\rho_0)^4 - (\gamma_0/2 - 2)(\rho/\rho_0)^2. \quad (1)$$
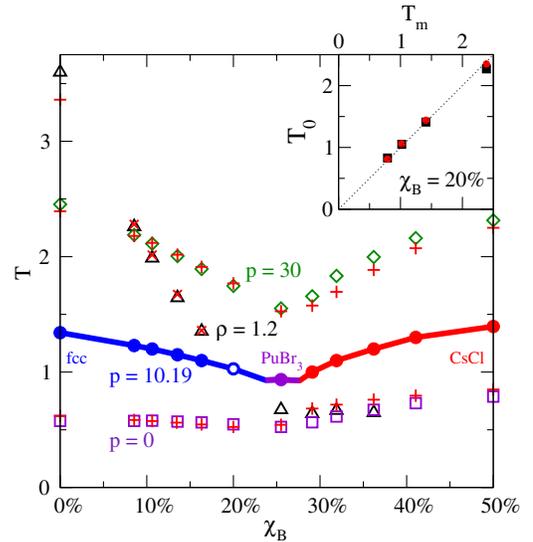
FIG. 4.   Isomorph-theory estimated melting temperature as a function of B particle concentration at fixed liquid-phase density $\rho = 1.2$ (triangles), as well as at pressures $p = 0$ and $p = 30$ (squares and diamonds). The circles connected by colored full lines are the results from Fig. 3, giving the reference states from which the open symbols are predicted. Red crosses are the actual melting temperatures. (Inset) Melting temperature T_m versus the onset temperatures T_0 (not to be confused with the above isomorph reference temperature), identified by Coslovich and Pastore at which the A and B particle dynamics (black and red) change from Arrhenius to non-Arrhenius temperature dependence [45]. The four points shown represent different densities (pressures) of the standard 80/20 KA model.

TABLE II. Thermodynamic quantities along the $p = 10.19$ melting line used for estimating the melting temperatures at constant liquid-phase density, as well as at two other pressures (Fig. 4).

χ_B	T_0	ρ_0	γ_0	u_0	w_0
0.000	1.341	0.980	5.16	−4.817	9.056
0.085	1.230	1.062	5.15	−5.256	8.372
0.106	1.200	1.084	5.11	−5.372	8.204
0.135	1.150	1.117	5.12	−5.548	7.971
0.163	1.100	1.151	5.10	−5.724	7.752
0.200	1.028	1.200	5.11	−5.974	7.444
0.255	0.935	1.278	5.10	−6.343	7.042
0.291	1.000	1.305	5.13	−6.354	6.808
0.319	1.100	1.316	5.18	−6.263	6.641
0.362	1.200	1.343	5.18	−6.202	6.384
0.410	1.300	1.375	5.19	−6.118	6.115
0.494	1.395	1.439	5.21	−5.953	5.691

FIG. 5. The crystal order parameter Q [36] plotted as a function of time averaged over 10^3 LJ time units. The blue crosses are from a fcc-liquid coexistence simulation at $T = 1.028$, and the red crosses are from a CsCl-liquid coexistence simulation at $T = 1$. These results indicate that the fcc interface is rough, whereas the CsCl interface is smooth and flat. The latter property impedes growth of the CsCl crystal. Particles with $Q_6 > 0.25$ are highlighted in the inserted coexistence pictures, where Q_6 is the rotational order parameter [38].

Here γ_0 is the density-scaling exponent at (ρ_0, T_0) computed from equilibrium, constant-density canonical-ensemble fluctuations via $\gamma_0 = \langle \Delta U \Delta W \rangle / \langle (\Delta U)^2 \rangle$, in which U is the potential energy and W is the virial [8]. At liquid density 1.2, the predictions based on Eq. (1) are shown as triangles in Fig. 4.

If one wishes to estimate from the $p = 10.19$ results the melting temperature at other pressures, the following procedure is employed. Along a LJ isomorph, the pressure varies as $p/\rho = k_B T + (2w_0 - 4u_0)(\rho/\rho_0)^4 - (w_0 - 4u_0) \times (\rho/\rho_0)^2$, in which w_0 and u_0 are the virial and potential energy per particle at the reference state point (ρ_0, T_0) [46]. Equation (1) is inserted into this expression, resulting in $p(\rho)/\rho = A(\rho/\rho_0)^4 - B(\rho/\rho_0)^2$, in which $A = k_B T_0(\gamma_0/2 - 1) + 2w_0 - 4u_0$ and $B = k_B T_0(\gamma_0/2 - 2) + w_0 - 4u_0$. This relation is inverted numerically and the melting temperature is estimated by inserting $\rho(p)$ into Eq. (1). The parameters used in the predictions are given in Table II.

The estimated melting temperature at $p = 0$ and $p = 30$ are shown in Fig. 4 as open squares and diamonds, respectively. These compare reasonably well to the actual melting temperatures (crosses). At the standard 80/20 composition, the zero-pressure melting temperature is estimated to be 0.547(8). The actual melting temperature is 0.525(4), which is 4% below the estimate. The largest deviation from the isomorph-theory estimated melting temperatures are found for the CsCl structure. In this case, there is a four times larger difference between the liquid and crystal density-scaling exponents than for the A particle fcc crystal, implying that the melting line is less accurately represented as an isomorph [39]. We note that for single-component systems, a more accurate melting-line theory exists based on a first-order Taylor expansion from the approximate melting isomorph [39].

By fitting relaxation times for the standard 80/20 KA system to the frustration-limited-domain theory of the glass transition [47], Coslovich and Pastore determined the "onset temperature" below which the non-Arrhenius temperature dependence of the relaxation time initiates [45]. The inset of Fig. 4 compares their data to the melting temperature at different pressures. There is good agreement, which tentatively confirms physical pictures of Sastry *et al.* [48,49] and Yanagishima *et al.* [50]. Though the identity of onset and melting temperatures may not apply universally, this suggests that a class of liquids exists for which it applies.

The two main crystal structures have different formation dynamics. Figure 5 shows how the crystal order parameter fluctuates at solid-liquid equilibrium. The coexisting fcc-liquid situation is more noisy than the CsCl-liquid case. We interpret the former as reflecting a rough interface, whereas in the latter case the interface is flat, i.e., grows layer by layer [51]. This is consistent with general findings [52] since the melting entropy is larger in the latter case (Table I).

In summary, we have mapped out the phase diagram of KA-type binary LJ mixtures showing, in particular, that the standard 80/20 KA liquid at density 1.2 crystallizes at $T = 1.028(3)$. Our findings suggest that KA systems more stable against crystallization are those of 26%–30% B particles. This is consistent with recent results of Ingebrigtsen and co-workers, who have simulated the density 1.2 KA viscous liquid with 25% and 33.33% B particles for months on a GPU cluster without being able to crystallize these systems [53].

*ulf@urp.dk

[1] N. Goldenfeld, *Lectures on Phase Transitions and the Renormalization Group* (Addison-Wesley, Reading, MA, 1992).

[2] M. Niss, Arch. Hist. Exact Sci. **59**, 267 (2005); **63**, 243 (2009); **65**, 625 (2011).

[3] D. J. Amit, *Field Theory, the Renormalization Group, and Critical Phenomena*, 3rd ed. (World Scientific, Singapore, 2005).

[4] A. Barrat, J. Kurchan, V. Loreto, and M. Sellitto, Phys. Rev. Lett. **85**, 5034 (2000).

[5] S. Franz, R. Mulet, and G. Parisi, Phys. Rev. E **65**, 021506 (2002).

[6] S. S. Ashwin and S. Sastry, J. Phys. Condens. Matter **15**, S1253 (2003).

[7] E. Flenner and G. Szamel, Phys. Rev. E **72**, 011205 (2005).

[8] N. Gnan, T. B. Schrøder, U. R. Pedersen, N. P. Bailey, and J. C. Dyre, J. Chem. Phys. **131**, 234504 (2009).

[9] U. R. Pedersen, T. B. Schrøder, and J. C. Dyre, Phys. Rev. Lett. **105**, 157801 (2010).

[10] W. Kob and H. C. Andersen, Phys. Rev. E **51**, 4626 (1995).

[11] L. O. Hedges, R. L. Jack, J. P. Garrahan, and D. Chandler, Science **323**, 1309 (2009).

[12] S. Toxvaerd, U. R. Pedersen, T. B. Schrøder, and J. C. Dyre, J. Chem. Phys. **130**, 224501 (2009).

[13] G. Wahnström, Phys. Rev. A **44**, 3752 (1991).

[14] U. R. Pedersen, T. B. Schrøder, J. C. Dyre, and P. Harrowell, Phys. Rev. Lett. **104**, 105701 (2010).

[15] C. Schmetterer, J. Vizdal, and H. Ipser, Intermetallics **17**, 826 (2009).

[16] Q. Zhang, K. De Oliveira Vigier, S. Royer, and F. Jerome, Chem. Soc. Rev. **41**, 7108 (2012).

[17] D. Turnbull, Contemp. Phys. **10**, 473 (1969).

[18] M. R. Hitchcock and C. K. Hall, J. Chem. Phys. **110**, 11433 (1999).

[19] M. H. Lamm and C. K. Hall, Fluid Phase Equilib. **182**, 37 (2001).

[20] M. H. Lamm and C. K. Hall, AIChE J. **47**, 1664 (2001).

[21] D. A. Kofke, J. Chem. Phys. **98**, 4149 (1993).

[22] T. F. Middleton, J. Hernandez-Rojas, P. N. Mortenson, and D. J. Wales, Phys. Rev. B **64**, 184201 (2001).

[23] M. Asta, C. Beckermann, A. Karma, W. Kurz, R. Napolitano, M. Plapp, G. Purdy, M. Rappaz, and R. Trivedi, Acta Mater. **57**, 941 (2009).

[24] J. R. Fernandez and P. Harrowell, Phys. Rev. E **67**, 011403 (2003).

[25] S. Jungblut and C. Dellago, J. Chem. Phys. **134**, 104501 (2011).

[26] R. Brüning, D. A. St-Onge, S. Patterson, and W. Kob, J. Phys. Condens. Matter **21**, 035117 (2009).

[27] P. Crowther, F. Turci, and C. P. Royall, J. Chem. Phys. **143**, 044503 (2015).

[28] U. K. Nandi, A. Banerjee, S. Chakrabarty, and S. M. Bhattacharyya, J. Chem. Phys. **145**, 034503 (2016).

[29] N. P. Bailey, T. S. Ingebrigtsen, J. S. Hansen, A. A. Veldhorst, L. Bøhling, C. A. Lemarchand, A. E. Olsen, A. K. Bacher, L. Costigliola, U. R. Pedersen, H. Larsen, J. C. Dyre, and T. B. Schrøder, SciPost Phys. **3**, 038 (2017).

[30] S. Plimpton, J. Comput. Phys. **117**, 1 (1995).

[31] W. Humphrey, A. Dalke, and K. Schulten, J. Mol. Graphics **14**, 33 (1996).

[32] http://urp.dk/tools.

[33] M. Parrinello and A. Rahman, J. Appl. Phys. **52**, 7182 (1981).

[34] G. J. Martyna, D. J. Tobias, and M. L. Klein, J. Chem. Phys. **101**, 4177 (1994).

[35] C. A. Becker, M. Asta, J. J. Hoyt, and S. M. Foiles, J. Chem. Phys. **124**, 164708 (2006).

[36] U. R. Pedersen, J. Chem. Phys. **139**, 104102 (2013).

[37] J. R. Fernandez and P. Harrowell, AIP Conf. Proc. **708**, 496 (2004).

[38] W. Lechner and C. Dellago, J. Chem. Phys. **129**, 114707 (2008).

[39] U. R. Pedersen, L. Costigliola, N. P. Bailey, T. B. Schrøder, and J. C. Dyre, Nat. Commun. **7**, 12386 (2016).

[40] U. R. Pedersen, N. P. Bailey, T. B. Schrøder, and J. C. Dyre, Phys. Rev. Lett. **100**, 015701 (2008).

[41] N. P. Bailey, U. R. Pedersen, N. Gnan, T. B. Schrøder, and J. C. Dyre, J. Chem. Phys. **129**, 184507 (2008).

[42] J. C. Dyre, J. Phys. Chem. B **118**, 10007 (2014).

[43] L. Bøhling, T. S. Ingebrigtsen, A. Grzybowski, M. Paluch, J. C. Dyre, and T. B. Schrøder, New J. Phys. **14**, 113035 (2012).

[44] T. S. Ingebrigtsen, L. Bøhling, T. B. Schrøder, and J. C. Dyre, J. Chem. Phys. **136**, 061102 (2012).

[45] D. Coslovich and G. Pastore, J. Chem. Phys. **127**, 124505 (2007).

[46] T. B. Schrøder, N. Gnan, U. R. Pedersen, N. P. Bailey, and J. C. Dyre, J. Chem. Phys. **134**, 164505 (2011).

[47] G. Tarjus, D. Kivelson, S. Mossa, and C. Alba-Simionesco, J. Chem. Phys. **120**, 6135 (2004).

[48] S. Sastry, P. G. Debenedetti, and F. H. Stillinger, Nature (London) **393**, 554 (1998).

[49] S. Sastry (unpublished).

[50] T. Yanagishima, J. Russo, and H. Tanaka, Nat. Commun. **8**, 15954 (2017).

[51] A. Pimpinelli and J. Villain, *Physics of Crystal Growth* (Cambridge University Press, Cambridge, England, 1998).

[52] K. A. Jackson, *Kinetic Processes* (Wiley-VCH, New York, 2004).

[53] T. S. Ingebrigtsen, J. C. Dyre, T. B. Schrøder, and C. P. Royall, arXiv:1804.01378.